Predictable irregularities in retinal receptive fields

Yuan Sophie Liu[a,b], Charles F. Stevens[c,1], and Tatyana O. Sharpee[a,b]

[a]Computational Neurobiology Laboratory and [c]Molecular Neurobiology Laboratory, The Salk Institute for Biological Studies, La Jolla, CA 92037; and [b]Center for Theoretical Biological Physics, University of California at San Diego, La Jolla, CA 92093

Contributed by Charles F. Stevens, August 10, 2009 (sent for review June 1, 2009)

Understanding how the nervous system achieves reliable performance using unreliable components is important for many disciplines of science and engineering, in part because it can suggest ways to lower the energetic cost of computing. In vision, retinal ganglion cells partition visual space into approximately circular regions termed receptive fields (RFs). Average RF shapes are such that they would provide maximal spatial resolution if they were centered on a perfect lattice. However, individual shapes have fine-scale irregularities. Here, we find that irregular RF shapes increase the spatial resolution in the presence of lattice irregularities from ≈60% to ≈92% of that possible for a perfect lattice. Optimization of RF boundaries around their fixed center positions reproduced experimental observations neuron-by-neuron. Our results suggest that lattice irregularities determine the shapes of retinal RFs and that similar algorithms can improve the performance of retinal prosthetics where substantial irregularities arise at their interface with neural tissue.

information theory | neural coding | optimal design | retina

Circuits in the nervous system, built from cells and the connections between them, cannot be made as regular as in the engineered man-made systems. Yet, animals can detect and act on signals in the environment with precision that not only rivals that of engineered systems, but also approaches the fundamental statistical limits set by the uncertainties in the environment itself. A classic example in the visual system is the detection of light under dim conditions, where the probability that a human would report seeing a flash of light equals the probability that a single photon would reach the retina (1). A parallel problem is how to arrange a set of detectors to best localize the position of a flash of light. Neurons in the retina respond to flashes of light localized to regions of visual space termed receptive fields (RFs). RFs of retinal ganglion cells, which send signals to the cortex, are arranged in an approximately hexagonal lattice, which allows for the densest packing of circles in two dimensions. Remarkably, the size of RFs increases proportionally with the distance L between neighboring RF centers, see *Quantification of Scatter in Receptive Field Center Positions in Experimental Mosaics* in supporting information (SI) *Text* and Fig. S1 for how it is derived. If RFs are described as Gaussians, then the width σ of the Gaussian is found to be $\approx L/2$ in different species and types of retinal ganglion cells (2–12) (Fig. 1*A*), with the exception of some cell types in the salamander retina (5). Furthermore, recent studies find that although individual RFs are approximately circular, there is interdigitation between neighboring RFs that is destroyed by a 180° rotation of individual RFs (13). Similar interdigitation has also been observed in dendritic fields (14). This suggests that RF shapes are adjusted locally and that deviations from circularity are functionally important. If so, understanding the best way to adjust response regions in an irregular array will also help improve the performance of retinal prosthetic devices (15).

Results

In this article, we consider how accurately the retina can represent the location of a point light source. Although this task is arguably one of the simplest in natural vision, it provides a good approximation of retinal function at low light levels. Under bright light, retinal ganglion cells become sensitive to contrast between nearby light intensities. Under these conditions, RFs can be described by a difference of two Gaussians that represent the average light intensity in the RF "center" and within the broader "surround" (see ref. 16 for a recent review). Because contrast values are much less strongly correlated in space than the light intensity values themselves, analysis of optimal RFs for detecting spots of light may be relevant for determining some of the properties of retinal RFs for detecting spots of contrast under bright light conditions.

To quantify the spatial resolution of the retina, we used two different measures. The first measure was the error between the actual location of a point light source and the best estimate of its location made on the basis of the array's responses. To estimate the location of a point light source, one can compare the set of observed responses of retinal cells with those expected for different light locations without knowing particular perturbations in either the neural responses or in the RF center locations. The location that provides the best match, in a least-square sense, to the data can be used to estimate the flash's origination point. Because the estimation error depends on how close the flash was to one of the RF centers, we were interested in its average value across different locations of the flash (see *Minimization of Average Square Error in Determining the Location of a Point Light Source* in *SI Text* and Fig. S2). One of the advantages of this measure is that it directly quantifies how accurately the retina can localize point light sources. In this computation, RFs were modeled as Gaussians. Retinal responses were assumed proportional to RF values taken at the spot's location, with additive Poisson noise that was independent between different cells and had the same coefficient of variation across all cells.

As the second measure for the retinal spatial resolution, we took the number of regions to within which a point light source can be localized based on retinal responses. For example, when two neighboring cells simultaneously respond to a flash of light, the flash is likely to have originated within the region of the visual space where the RFs of the two cells overlap. If three cells simultaneously respond, this further constrains the likely origination region. Even when the third neighboring cell does not respond to the flash, this nevertheless is informative because it shifts the likely origination point away from the nonresponding cell. Such simple arguments illustrate the power of combinatorial coding available to the retinal array. The number of distinct regions N_d can be computed using information theory: $N_d = 2^I$, where I is the mutual Shannon information (17) between the responses of neurons in the array and the location of a point light source. The main motivation for using information-theoretic quantities in this context is that they can quantify how combi-

Author contributions: C.F.S. and T.O.S. designed research; Y.S.L., C.F.S., and T.O.S. performed research; Y.S.L., C.F.S., and T.O.S. analyzed data; and Y.S.L., C.F.S., and T.O.S. wrote the paper.

The authors declare no conflict of interest.

Freely available online through the PNAS open access option.

[1]To whom correspondence should be addressed. E-mail: stevens@salk.edu.

This article contains supporting information online at www.pnas.org/cgi/content/full/0908926106/DCSupplemental.

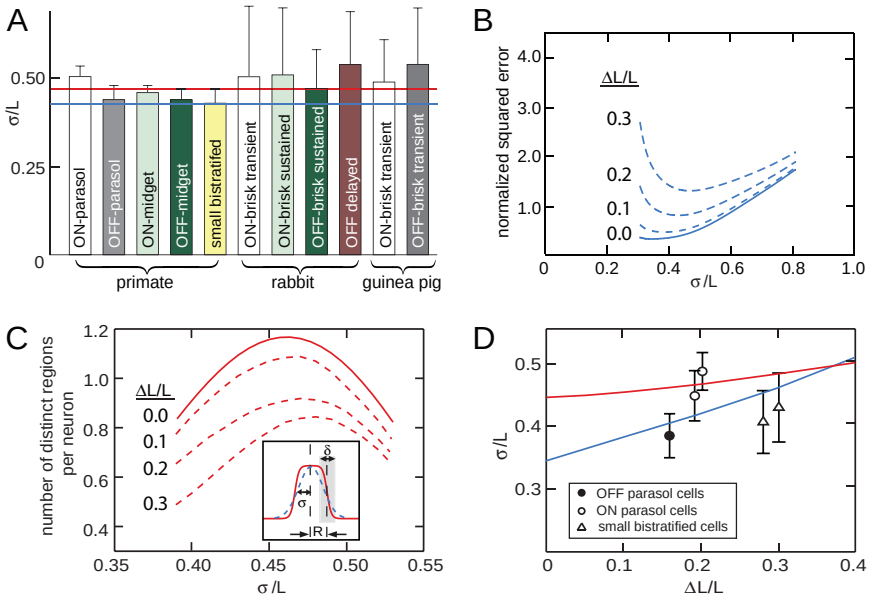

Fig. 1. Properties of retinal ganglion cell mosaics with circular receptive fields in the presence of lattice irregularities. (*A*) Average receptive field size for ganglion cells of different classes and species (2, 8–10, 12) is consistent with predictions based on minimal square error (blue line) and information maximization (red line) obtained by averaging predictions for $0 < \Delta L/L < 0.4$, see *D*. (*B*) Mean-square error as a function of σ for mosaics with different average scatter in RF center position $\Delta L/L$ (see *Minimization of Average Square Error in Determining the Location of a Point Light Source* in *SI Text* for a derivation). (*C*) Predictions based on maximizing information *I* are plotted in terms of $n_d = 2^I/N$ as a function of σ of the best-fitting Gaussian. RF profiles themselves are not Gaussian. The *Inset* schematic shows parameters *R* and δ of the RF profile in the decision boundary approximation relative to the best-fitting Gaussian of width σ. (*D*) Optimal RF size for minimizing error (blue) or maximizing information (red) increases with scatter in RF center positions, in agreement with measurements from ref. 8.

natorial representations can improve the spatial resolution. Our goal here is to determine such mosaic properties that would maximize the number of distinct regions $n_d = N_d/N$ per neuron, where N is the number of neurons in the mosaic.

To understand the impact that different types of irregularities have on retinal function, we make our arguments in five steps. The first step is to analyze the case where RF center positions form a perfect hexagonal lattice. Here, our goals are to find the optimal size of individual RFs based on minimizing the mean-square error or maximizing the number of distinct regions, and to compare the optimal RF size with previous predictions made according to a number of other optimization criteria (10, 18–20). Next, we will analyze how the retinal performance is affected by lattice irregularities alone, with no asymmetries or variations in RF shapes across neurons. In the third step, we will briefly examine the performance of retinal mosaics where RF center positions form a regular lattice, whereas RF shapes vary from neuron to neuron. The fourth step is to consider the combined effect of irregularities in the lattice of RF center positions and irregularities in the individual RF shapes to show that the former predetermines the latter in retinal arrays. In this way, irregular arrays such as those observed in the retina can achieve a near-perfect performance. Finally, in the last step, we consider fine-scale adjustments in RF shapes to demonstrate that they can yield further improvements in information transmission, as well as reproduce the shapes of experimentally measured RFs (13).

Ideal RF Array. As one might expect, given an ideal array where RF centers form a regular hexagonal lattice (Fig. S3), the optimal shape of individual RFs is circular (18). As a function of RF size, there is a clear optimum in terms of both the minimal error and the maximal number of distinguishable regions for the light source n_d (solid lines in Fig. 1 *B* and *C*). When described in terms of the best-fitting Gaussian, the smallest error is obtained when $\sigma \approx 0.35L$ (see *Minimization of Average Square Error in Determining the Location of a Point Light Source* in *SI Text*), whereas the largest n_d is obtained when $\sigma \approx 0.45L$ (see *Information Transmission by a Retinal Array* in *SI Text*). In the case of information calculation (see *Materials and Methods*), we modeled RFs using the decision boundary approximation (21). In this approximation, RFs are described as two-dimensional sigmoidal functions based on two parameters: a radius *R* that corresponds to the half-width at half-maximum of the RF profile and a width δ of the sigmoid (Fig. 1*C Inset*). Although increasing δ lowered the information, it did not strongly affect the location of the information maximum as a function of RF size *R* (Fig. S4). For comparison with experimental data and predictions based on the mean square error, we fitted the sigmoidal RF profiles with Gaussians (Fig. 1*C Inset*; $\sigma \approx 0.67R$). Taken together, these analyses of the mean-square error based on Gaussian RFs and of the information based on sigmoidal RFs indicate that predictions for the optimal RF size are insensitive to changes in the functional form used to model the RF profiles.

The predicted optimal RF size is also advantageous according to a number of other computational measures, such as achieving maximally uniform contrast sensitivity (2), equal accuracy in detecting light whether it falls near a RF center or at an intermediate position (10), and maximizing information about scenes from the natural environment (10, 18–20). In summary then, even though all of the above analyses ignore irregularities present in real retinal arrays, they all can account for the experimentally observed increase in the average RF size σ with lattice spacing L, indicating that such a scaling relationship might be functionally advantageous from multiple computational perspectives.

Irregular Mosaics of Circular RFs. Proceeding to the second step, we now analyze how the retinal performance is affected by lattice irregularities alone. The degree of lattice irregularity will be quantified according to the standard deviation ΔL of RF center positions compared to the regular hexagonal lattice (see *Quantification of Scatter in Receptive Field Center Positions in Exper-*

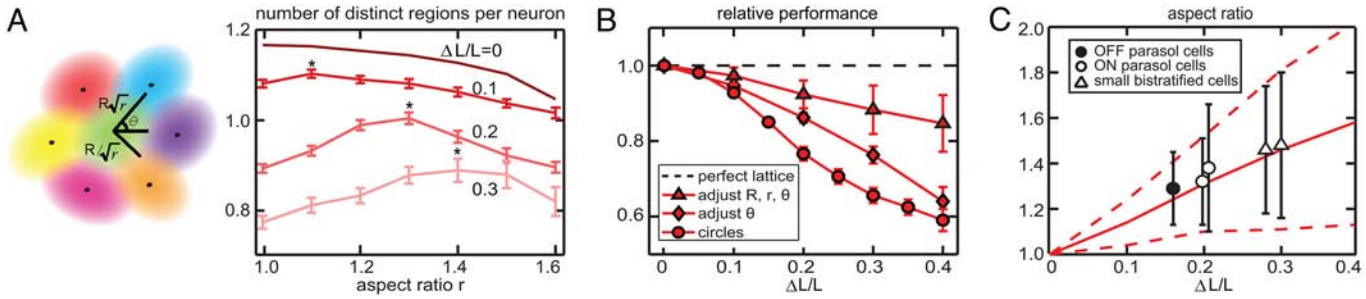

Fig. 2. Adjustments in RF shapes compensate for scatter in RF center positions. (*A*) Elliptical RFs yield larger number of regions that can be distinguished based on retinal responses. Schematic shows parameters of the elliptic model for RF profiles: aspect ratio r, orientation θ relative to the horizontal axes, and the geometric average R of the semimajor $R\sqrt{r}$ and the semiminor $R/\sqrt{r}$ axes (ellipse area is πR^2). Luminance describes the probability of a spike in a given neuron to point light source at different spatial locations; RFs were modeled in decision boundary approximation with $\delta = 0.23R$. Aspect ratios were the same for all neurons in a mosaic. Stars mark the optimal aspect ratio in each curve, the value of the maximum was significantly larger than that for $r = 1$ for each of the curves (t test, $P \leq 0.01$). (*B*) Adjustments of elliptical RFs increase the performance in the presence of center position scatter. The number of distinguishable regions is given relative to that maximally attainable with a regular hexagonal array of circular RFs (dashed line). Scatter in RF center positions progressively decreases performance with circular RFs (○). This decrease can be counteracted by using elliptical RFs whose size, aspect ratio, and orientation are adjusted individually for each neuron (Δ). The improvement is smaller when only the orientation, but not the aspect ratio and size, are adjusted individually (◇). In the latter case, the aspect ratio was set to the optimal value determined from *B*. (*C*) Statistics of aspect ratio values of optimized mosaics agree with experimental data. Mean (solid line) ± standard deviations (dashed) of aspect ratios found in optimized mosaics from *B*. Data are extracted from mosaics in refs. 8 and 9.

imental Mosaics in *SI Text* for how ΔL was determined in experimental mosaics). As might be expected, the mean-square error (Fig. 1*B*) increases with increasing scatter in RF center positions. Similarly, the number of distinct regions (Fig. 1*C*) decreases with increasing center position scatter.

Over the range of $\Delta L/L$ values typical of experimental mosaics, the predictions vary within a narrow range centered at $\approx 0.45L$. The narrow width of this range explains why predictions made by using various optimization criteria assuming a regular lattice are in such good agreement with experimental data (10, 18–20) (Fig. 1*A*). However, a more detailed analysis of either the mean-square error (Fig. 1*B*) or the number of distinct regions (Fig. 1*C*) predicts an increase in the optimal RF size with an increasing amount of scatter in RF center positions. In Fig. 1*D*, we show that the predicted increase in the RF size from $\approx 0.35L$ to $\approx 0.5L$ over the experimentally observed range of center position scatter captures the basic trend exhibited by experimental data. Thus, a large scatter in RF center positions can be compensated by increasing the RF size, a result that holds both for error minimization and information maximization.

Mosaics of Evenly Spaced Elliptical RFs. The third situation is where elliptical RF shapes are centered on a regular hexagonal lattice. Here, the deviations from circularity in RF shapes progressively deteriorate the performance of a retinal mosaic (Fig. 2*A*, top curve). In these simulations, we approximated RF boundaries as ellipses and used a decision boundary approximation to compute the number of distinct regions for the light source (see *Mosaic with center position scatter* in *SI Text*). All RFs in the mosaic had the same aspect ratio (see schematic in Fig. 2*A* for parameter definitions), whereas the orientation of individual RFs was adjusted individually to optimize performance of the array as a whole. Despite this optimization, the larger the aspect ratio was, the smaller the number of regions that could be distinguished based on the array's responses. The same effect was true of the uniformity of coverage (13). Thus, both the RF shape and lattice irregularities are detrimental to retinal performance when considered separately.

Mosaics of Elliptical RFs Centered on an Irregular Lattice. In contrast, in the fourth case where both the lattice and RF shapes have irregularities, we found elliptical RFs (with aspect ratio >1) to be beneficial (Fig. 2*A*, lower curves). Although mosaics of elliptical RFs encoded fewer distinct regions for the point light source (Fig. 2 *A* and *B*) than the optimal mosaic with no lattice irregularities, this number was greater than that where RFs were constrained to be circular in the presence of lattice irregularities. For a given amount of average scatter in RF center positions, there was an optimal value of RF aspect ratio that increased with the amount of center position scatter (Fig. 2*A*). The intuition for this finding is that when two RF centers are a bit further from each other than from their other neighboring neurons, elliptical RFs allow for an increase in the amount of overlap between the more distant pair without a large change in overlap with other cells.

In a retinal array, RFs vary not only in their orientation, but also in their aspect ratio and size. We found that the mosaic performance improved even more when the orientation, aspect ratio, and size could be adjusted neuron-by-neuron (Fig. 2*B*). With adjustable size, aspect ratio, and orientation, elliptical RFs could restore ≈75% of the number of distinct patterns lost due to irregularities in RF centers. For the degree of scatter typical of parasol ($\Delta L \approx 0.2L$) and small-bistratified ($\Delta L \approx 0.3L$) mosaics, mosaics of circular RFs could encode only ≈60% of the number of positions that can be represented in a perfect lattice, whereas mosaics of elliptical RF can represent as much as ≈90% of that number.

Optimized mosaics had a distribution of aspect ratios that is very similar to those observed experimentally. In particular, we found that the mean aspect ratio was larger in mosaics with greater amounts of scatter in the RF center positions (Fig. 2*C*). In addition, the standard deviation of aspect ratios across a mosaic also increased with RF center position scatter. This correlation was in full agreement with measurements on real retinal mosaics (Fig. 2*C*). For example, arrays of small bistratified cells (8, 9), which are more irregular than mosaics of parasol cells, not only have RFs with larger mean aspect ratio than those of parasol cells but also a greater variance in the aspect ratios across RFs in a mosaic. Thus, maximizing the number of regions that could be reliably distinguished based on the responses of the retinal array (or, equivalently, the mutual information about the location of a point light source) can account for the average statistical properties of RF shapes in different types of retinal cells.

Could this optimization criterion also reproduce the local structure of experimentally measured mosaics? To test this, we optimized the orientation, aspect ratio, and size of individual RFs whose centers were fixed to the same relative positions as in experimentally recorded mosaics. We found that after just a

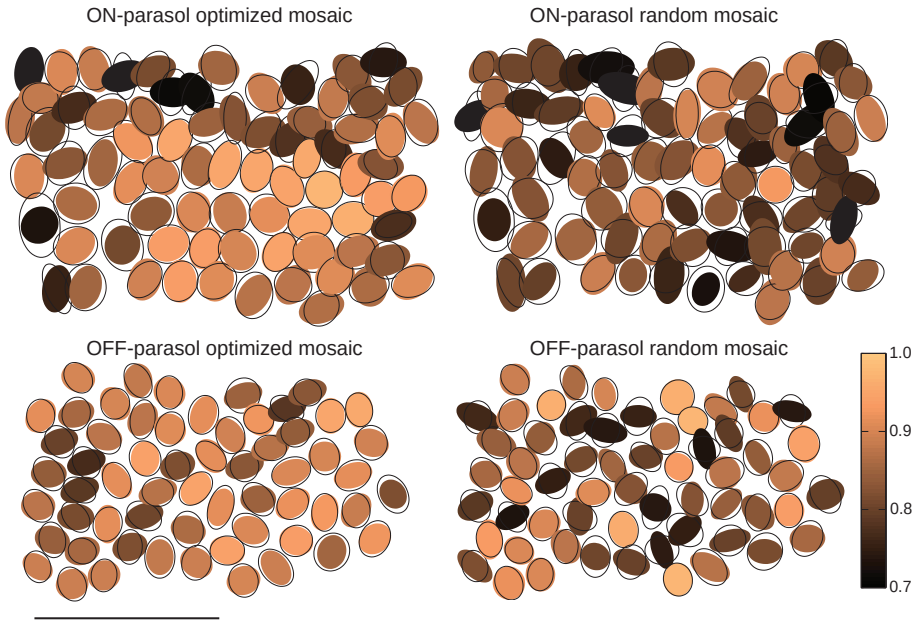

Fig. 3. Irregularities in lattice spacing determine RF shapes in retinal mosaics. Empty ellipses show retinal mosaics from ref. 8 that were drawn at 1.3 standard deviations of a Gaussian fit. Colored ellipses represent the corresponding contour levels of best-fitting Gaussians to RF profiles of the optimized mosaic. During optimization, orientation, aspect ratio, and RF size were adjusted individually, whereas RF centers coincided with those in the experimental mosaics. After optimization, theoretical RFs were rescaled by a factor 1.1 and 1.2 in ON- and OFF-parasol mosaics to match the average RF size in experimental mosaics. Color shows the correlation coefficient between theoretical and experimental RFs. The match is particularly good for neurons in the middle of a mosaic and was significantly better than that for mosaics where RF size, orientation, and aspect ratio were selected at random (*Right*; $P < 0.002$) as opposed to optimized (*Left*). (*Upper*) ON-parasol cells. (*Lower*) OFF-parasol cells. (Scale bar, 1 mm.)

few rounds of optimization in which the parameters of individual RFs were adjusted sequentially while keeping those of neighboring RFs fixed, the optimization had converged to the mosaic that closely matched the experimental one. In particular, the local mosaic structure was accounted for on a neuron-by-neuron basis (Fig. 3). The results were independent of the sequence in which RF shapes were optimized (Fig. S5). The average correlation coefficients between predicted and experimental RFs were 0.86 and 0.87 for mosaics of on- and off-parasol cells, respectively. These values were significantly larger than those obtained when the size, aspect ratio, and orientation of RFs was selected at random (0.81 and 0.83, $P < 0.002$, t test). In general, the match between experimental and model mosaics was particularly good for cells in the middle of the mosaic. Presumably, this was because the RFs of cells near an edge or a gap in the mosaic were under-constrained due to the exclusion of neighboring cells. In summary then, we find that irregularities of RF shapes can be predicted based on irregularities of spacing and that they can largely compensate for the decrease in the resolution of a retinal array that would be expected based on spacing irregularities alone.

Predicting Fine-Scale Irregularities in RF Shapes. Although elliptical approximation captures the most prominent features of retinal RF boundaries, the real RFs also have a fine scale structure that can improve their tiling (13). However, there are multiple ways to uniformly tile the visual space. Therefore, in our last step, we consider whether optimizing RF boundaries to maximize the number of distinguishable regions in the visual space can also reproduce the fine-scale structure of a particular experimentally measured mosaic. To model irregularities in RF shapes, we represented them using linear combinations of Legendre polynomials $P_n(\cos(\theta/2))$ of orders $n \leq 10$. Legendre polynomials form a complete set and, therefore, could describe an arbitrary shape provided that a sufficient number of terms are included. We found that the optimization of irregular RF shapes around the best-fitting elliptical shape produced boundaries that closely matched experimental data, see Fig. 4*A*. The match between optimized and experimental shapes was significantly better than that for a randomly selected set of Legendre coefficients within the optimized range ($P < 0.005$, both shapes had the same parameters of the best-fitting ellipse). Of course, variations in RF shape that affect neither the length of RF boundaries (a measure of neural noise, see *Mosaic with center position scatter* in *SI Text*) nor the probabilities of different response patterns across the retina cannot be distinguished in this approach. However, predictions can be made with respect to the probabilities of observing various patterns of neural responses (see *Materials and Methods*). In Fig. 4*B*, we compare the probabilities of observing different spike patterns for the experimental and the optimized theoretical mosaic. The probabilities closely match on a pattern-by-pattern basis. The correlation coefficient, $R = 0.995$, is significantly better than that obtained for a control mosaics where Legendre coefficients were selected at random from the same distribution as in the optimized mosaics ($P < 10^{-6}$). Finally, this fine-scale optimization of RF shapes increased the relative performance of this mosaic from ≈89% in the elliptical approximation to ≈92% of the possible maximum. Thus, optimizing shapes of individual RFs in an irregular mosaic to maximize the number of distinguishable regions in the visual space can account for both average statistical properties of retinal mosaics and the fine-scale irregularities in the shapes of individual RFs.

Discussion

These analyses demonstrate that although asymmetries in individual retinal RFs would be detrimental when considered individually, when considered as part of a retinal circuit, these asymmetries actually help irregular arrays achieve ≈92% of the representational capacity of a fully regular optimal array. This

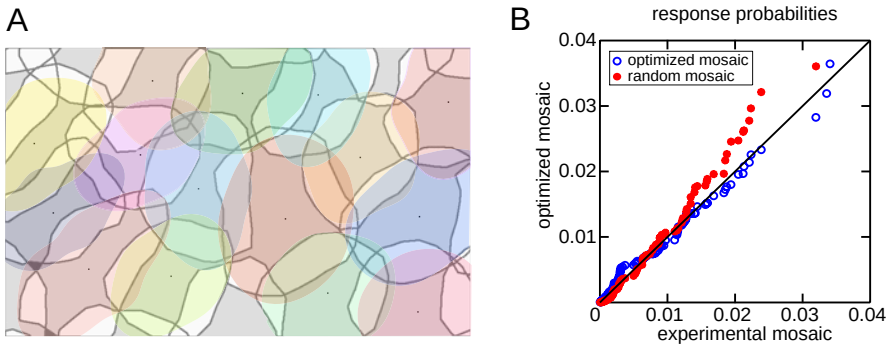

Fig. 4. Accounting for fine-scale irregularities in RF shapes based on RF center positions. (*A*) Gray contours are data from ref. 13. Starting from the best-fitting ellipses, shapes of neural RFs were optimized further to allow for shape irregularities through expansion in Legendre polynomials (see *Mosaic with center position scatter* in *SI Text*). The image width is 660 μm. (*B*) The probability of occurrence of each pattern of the array's responses computed from the optimized mosaic is plotted against those computed from the measured mosaics. Each circle stands for one of the 108 possible binary activity patterns for a mosaic of 15 cells in *A*. Blue empty circles: optimized mosaic, red: mosaic of RFs where coefficients in the Legendre expansion were selected at random from a Gaussian distribution with the same mean and variance as in the optimized mosaic.

happens because asymmetries in the RFs of individual cells can better coordinate the responses of individual cells so as to take full advantage of the combinatorial power available in an array's responses. Given the great flexibility in RF shape that can be achieved in the retina, one might wonder why RF shape and center position are not adjusted together to form a perfect hexagonal mosaic. The answer might be that because mosaics of cell bodies are established before (and largely without) dendritic contacts between neighboring cells (22), the anatomic and metabolic costs for adjusting RF shape might be less that those for displacing the RF center. Although, in principle, it is also possible to move a RF center by directing all of cell's dendrites in one direction, in practice, the correlation between a cell body position and the center of its RF is quite strong (23, 24). From a functional standpoint, our results indicate that there is almost no benefit from achieving a perfect mosaic—an irregular mosaic with appropriately adjusted asymmetric RF fields can be just as accurate in representing light positions.

Intriguingly, similar findings are observed for random packings of solid objects: Whereas regularly packed spheres allow for the densest packing, randomly packed ellipsoids (such as M&M milk chocolate candies) achieve higher densities than randomly packed spheres (25). This connection is more than superficial, because the problem of finding error-corrective codes can be mapped onto a packing problem of solid objects in high-dimensional spaces (26).

The problem of how to best partition the visual space given an irregular array is also relevant to the design of retinal prosthetic devices (15). The goal of these devices is to restore vision in patients who have lost their photoreceptor cells but where at least some fraction of retinal ganglion cells remain functional. Such a situation occurs in age-related macular degeneration or retinitis pigmentosa, two diseases that together cause blindness in millions of people worldwide (27–29). Retinal implants use a video camera as a replacement for photoreceptors in transducing light patterns and an array of electrodes positioned near the retina used to deliver electrical signals based on the camera output to the remaining ganglion cells. Even though the electrode array is regular, the recipient retinal ganglion cells shift their position after the death of photoreceptors (30). This introduces substantial irregularities at the brain–prosthesis interface. These irregularities can nevertheless be measured by asking patients to report the location of a perceived light flash after stimulation of individual electrodes of the implanted arrays (15). Although these irregularities are on a much larger scale than those observed for RF centers of ganglion cells in a healthy retina, our results suggest that an optimization of "RF boundaries" associated with each electrode can partially compensate for the irregularities in the percepts positions elicited by electrode stimulation. The optimization procedure we described here can be carried on any scale, and thus can be used to increase the spatial resolution of the implant by tuning it to the particular distribution of perceptual irregularities.

Materials and Methods

The computation of mutual information between the responses of retinal cells and the location of a spot of light consists of two steps (17). The first step is to compute the "response" entropy based on the probabilities to observe various patterns of retinal responses averaged across possible positions of the light spot. The second step is to compute the "noise" entropy based on response probabilities for a given spot position. In the first step, one technically needs to take into account all possible combinations of spiking and silence of neurons in the mosaic. The number of these combinations increases exponentially with the number of neurons N in the mosaic. However, for the problem of spot detection that we consider here, the probability that a spot of light will elicit coincident spiking from neurons in widely separated regions of the mosaic is small, if not negligible. To speed up the computation of commonly occurring spike combinations, and to discard those that are extremely rare, we modeled RFs during information calculations as two-dimensional sigmoid functions (Fig. 1*C Inset*). The RF boundaries were defined as contour levels at 50% of the maximum. The spike probability (in a small time bin so that responses are binary) was assumed to be close to 1 or 0, depending on whether the light fell within or outside the RF boundary, and $\approx$0.5 whenever the light fell within the distance δ from the RF boundary. With these assumptions, the probability of observing a given spike pattern can be computed based on the area that is simultaneously covered by RFs of all spiking neurons and not covered by RFs of all nonspiking neurons in the response pattern under consideration. The normalization by the overall area covered by the mosaic then yields the probability of observing the corresponding pattern averaged across all positions of the light spot. In the second step of the information calculation, we assume that the noise in the retinal responses is Poisson, with mean rate proportional to RF, and independent across neurons. Given that the uncertainty in neural responses is the largest for spots of light falling near RF boundary, the average entropy in the retinal responses can be approximated as proportional to width δ of RF boundary and the total length of all RF boundaries in the mosaic. For further details of the computation, see *Information Transition by a Retinal Array* in *SI Text*.

ACKNOWLEDGMENTS. We thank William Bialek, E. J. Chichilnisky, Greg Field, Jeff Gauthier, and Jeff Fitzgerald for useful discussions; Vijay Balasubramanian and Leo van Hemmen for suggestions and comments on the manuscript; and Terrence Sejnowski for initiating our collaboration. This work was supported by a Pioneer Postdoctoral fund (to Y.S.L.) and National Science Foundation Grant IIS-0712852 (to T.O.S.). T.O.S. was also supported by an Alfred P. Sloan Fellowship, Searle Scholarship, National Institute of Mental Health Grant K25MH068904, the Ray Thomas Edwards Career Development Award in Biomedical Sciences, the McKnight Young Scholar Award, and the Research Excellence Award from the W. M. Keck Foundation.

1. Rieke F, Warland D, de Ruyter van Steveninck RR, Bialek W (1997) *Spikes*: *Exploring the Neural Code* (MIT Press, Cambridge, MA).
2. Devries SH, Baylor DA (1997) Mosaic arrangement of ganglion cell receptive fields in rabbit retina. *J Neurophysiol* 78:2048–2060.
3. Chichilnisky EJ, Kalmar RS (2002) Functional asymmetries in on and off ganglion cells of primate retina. *J Neurosci* 22:2737–2747.
4. Chichilnisky EJ, Kalmar RS (2003) Temporal resolution of ensemble visual motion signals in primate retina. *J Neurosci* 23:6681–6689.
5. Segev R, Puchalla J, Berry II MJ (2005) Functional organization of ganglion cells in the salamander retina. *J Neurophysol* 95:2277–2292.
6. Frechette ES, et al. (2005) Fidelity of the ensemble code for visual motion in primate retina. *J Neurophysol* 94:119–135.
7. Shlens J, et al. (2006) The structure of multi-neuron firing patterns in primate retina. *J Neurosci* 26:8254–8266.
8. Field GD, Chichilnisky EJ (2007) Information processing in the primate retina: Circuitry and coding. *Annu Rev Neurosci* 30:1–30.
9. Field GD, et al. (2007) Spatial properties and functional organization of small bistratified ganglion cells in primate retina. *J Neurosci* 27:13261–13272.
10. Borghuis BG, Ratliff CP, Smith RG, Sterling P, Balasubramanian V (2008) Design of a neuronal array. *J Neurosci* 28:3178–3189.
11. Lee S, Stevens CF (2007) General design principle for scalable neural circuits in a vertebrate retina. *Proc Natl Acad Sci USA* 104:12931–12935.
12. Gauthier JL, et al. (2009) Uniform signal redundancy of parasol and midget ganglion cells in primate retina. *J Neurosci* 29:4675–4680.
13. Gauthier JL, et al. (2009) Receptive fields in primate retina are coordinated to sample visual space more uniformly. *PLoS Biol* 7(4):e1000063.
14. Wassle H, Peichl L, Boycott BB (1981) Dendritic territories of cat retinal ganglion cells. *Nature* 292:344–345.
15. Humayun MS, et al. (2003) Visual perception in a blind subject with a chronic microelectronic retinal prosthesis. *Vis Res* 43:2573–2581.
16. Balasubramanian V, Sterling P (2009) Receptive fields and functional architecture in the retina. *J Physiol* 587:2753–2767.
17. Cover TM, Thomas JA (1991) *Information Theory* (Wiley, New York).
18. Haft M, van Hemmen JL (1998) Theory and implementation of infomax filters for the retina. *Netw Comput Neural Syst* 9:39–71.
19. Atick JJ, Redlich AN (1990) Towards a theory of early visual processing. *Neural Comput* 2:308–320.
20. Doi E, Lewicki MS (2007) A theory of retinal population coding. *Advances in Neural Information Processing*, eds Schölkopf B, Platt JC, Hoffman T (MIT Press, Cambridge, MA), Vol 19, pp 353–360.
21. Sharpee TO, Bialek W (2007) Neural decision boundaries for maximal information transmission. *PLoS One* 2:e646.
22. Lin B, Wang SW, Masland RH (2004) Retina ganglion cell type, size, and spacing can be specified independent of homotypic dendritic contacts. *Neuron* 43:475–485.
23. Peichl L, Wassle H (1983) The structural correlate of the receptive field centre of alpha ganglion cells in the cat retina. *J Physiol* 341:309–324.
24. Wassle H, Peichl L, Boycott BB (1983) A spatial analysis of on- and off- ganglion cells in the cat retina. *Vis Res* 23:1151–1160.
25. Donev A, et al. (2004) Improving the density of jammed disordered packings using ellipsoids. *Science* 303:990–993.
26. Thompson TM (1983) From error correcting codes through sphere packings to simple groups (Mathematical Assoc of America, Washington, DC).
27. Chong NH, Bird AC (1999) Management of inherited outer retinal dystrophies: present and future. *Br J Ophthalmol* 83:120–122.
28. Sharma RK, Ehinger B (1999) Management of hereditary retinal degenerations: Present status and future directions. *Surv Ophthalmol* 43:427–444.
29. Friedman DS, et al. (2004) Prevalence of age-related macular degeneration in the united states. *Arch Ophthalmol* 122:564–572.
30. Marc RE, Jones BW, Watt CB, Strettoi E (2003) Neural remodeling in retinal degeneration. *Progr Retinal Eye Res* 22:607–655.